AIP Journal of Applied Physics

Kinetics of the B1-B2 phase transition in KCl under rapid compression

Chuanlong Lin, Jesse S. Smith, Stanislav V. Sinogeikin, Changyong Park, Yoshio Kono, Curtis Kenney-Benson, Eric Rod, and Guoyin Shen

Citation: Journal of Applied Physics **119**, 045902 (2016); doi: 10.1063/1.4940771
View online: http://dx.doi.org/10.1063/1.4940771
View Table of Contents: http://scitation.aip.org/content/aip/journal/jap/119/4?ver=pdfcov
Published by the AIP Publishing

JOURNAL OF APPLIED PHYSICS **119**, 045902 (2016)

Kinetics of the B1-B2 phase transition in KCl under rapid compression

Chuanlong Lin, Jesse S. Smith, Stanislav V. Sinogeikin, Changyong Park, Yoshio Kono, Curtis Kenney-Benson, Eric Rod, and Guoyin Shen[a)]
HPCAT, Geophysical Laboratory, Carnegie Institution of Washington, Argonne, Illinois 60439, USA

(Received 1 August 2015; accepted 14 January 2016; published online 28 January 2016)

Kinetics of the B1-B2 phase transition in KCl has been investigated under various compression rates (0.03–13.5 GPa/s) in a dynamic diamond anvil cell using time-resolved x-ray diffraction and fast imaging. Our experimental data show that the volume fraction across the transition generally gives sigmoidal curves as a function of pressure during rapid compression. Based upon classical nucleation and growth theories (Johnson-Mehl-Avrami-Kolmogorov theories), we propose a model that is applicable for studying kinetics for the compression rates studied. The fit of the experimental volume fraction as a function of pressure provides information on effective activation energy and average activation volume at a given compression rate. The resulting parameters are successfully used for interpreting several experimental observables that are compression-rate dependent, such as the transition time, grain size, and over-pressurization. The effective activation energy (Q_{eff}) is found to decrease linearly with the logarithm of compression rate. When Q_{eff} is applied to the Arrhenius equation, this relationship can be used to interpret the experimentally observed linear relationship between the logarithm of the transition time and logarithm of the compression rates. The decrease of Q_{eff} with increasing compression rate results in the decrease of the nucleation rate, which is qualitatively in agreement with the observed change of the grain size with compression rate. The observed over-pressurization is also well explained by the model when an exponential relationship between the average activation volume and the compression rate is assumed. © *2016 AIP Publishing LLC*. [http://dx.doi.org/10.1063/1.4940771]

I. INTRODUCTION

Understanding kinetics of phase transitions under high pressure is fundamental in condensed matter physics, and essential for synthesis of new materials, controlling chemical reactions, exploring material metastability, and understanding the dynamic nature of planetary interiors. High-pressure experimental science generally consists of static and dynamic experiments. Dynamic compression, until recently, mainly focuses on shock experiments with extremely high compression rates, while the compression rate of static experiments is usually very small. The influence of intermediate compression rates, between the typical static compression and shock compression rates, on materials is largely unexplored for most phase transformations.[1–10] For rapid compression, i.e., with the intermediate compression rates, it is crucial to have an apparatus that can combine various compression rates with *in situ* measurements on short time scales. Recently, the developments of dynamic diamond anvil cells (dDAC)[1,11–13] and high-frequency area detectors (e.g., Dectris' PILATUS and EIGER detectors)[14] have provided the possibility to study the kinetics and mechanism of phase transformations under various compression rates with time scales on the order of a millisecond. The use of dDACs allows studying various rate-dependent phenomena (or processes) such as compression-rate dependent phase transition pathways, crystal nucleation and growth, formation of metastable phases, and solidification of liquid.[1–3,8–10] Here, we chose potassium chloride (KCl) to study the kinetics of the B1-B2 phase transition at various compression rates using a dDAC[13] and time-resolved x-ray diffraction techniques[14] recently developed at the High Pressure Collaborative Access Team (HPCAT) at the Advanced Photon Source, Argonne National Laboratory.

The B1 (sodium chloride structure) to B2 (cesium chloride structure) phase transition of KCl is a classical reconstructive phase transition with a volume collapse of ~12% and has been studied extensively using both static high-pressure[15–20] and shock-wave techniques.[21–24] Corresponding phase transition mechanisms have been identified to describe the B1 to B2 phase transition. In static experiments, Hamaya and Akimoto[15] studied the kinetics of the B1-B2 phase transformation in KCl at constant over-pressurization levels. They found that the nuclei of the high-pressure B2 phase formed on the grain boundary and surface in the relatively low over-pressure range, while nuclei formed in the grain interior in the large over-pressure range, i.e., the nucleation mechanism changes from heterogeneous nucleation under low over-pressurization to homogeneous nucleation under high over-pressurization. In shock experiments, a high-speed dislocation mechanism was suggested for the shock-induced B1-B2 phase transition.[25,26] In that model, the shock-induced shear stress yields dislocation of the initial lattice B1 which results in the development of an intermediate structure with subsequent transformation into the final lattice B2.[25] Although many studies have been done on the mechanism of the B1-B2 phase transition in the contexts of both static compression and shock-wave experiments, there are no

[a)]Author to whom correspondence should be addressed. Electronic mail: gshen@ciw.edu

experimental data or theoretical models which explore the mechanism of the B1-B2 phase transition at intermediate compression rates between static and shock compression. The purpose of this work is, therefore, to fill the gap between two extremes with the newly developed rapid compression and time-resolved x-ray diffraction techniques and provide a better insight into the pressure-induced phase transition kinetics.

In a phase transition, the transition kinetics strongly depends on the activation energy.[27–29] Various properties and processes such as nucleation rate and growth rate are directly connected with the activation energy barriers which the system must overcome from metastable to stable state. At constant pressure (P) and temperature (T), the activation energies for the formation of nucleation (Q_N) and grain growth (Q_G) are time independent, and the rate constant of the phase transformation can be characterized by the Arrhenius equation[27,29,30]

$$1/\tau \sim \text{rate constant} = C_0 \exp\left[-Q/k_B T\right], \quad (1)$$

where Q is the activation energy in the nucleation and growth process at P and T; k_B is the Boltzmann constant; C_0 is a material dependent constant; τ is the characteristic time of the phase transformation. In KCl, the transition time scale can change from at least 4 h at 1.95 GPa to less than half an hour at 2.13 GPa.[15] The activation energy was estimated to be 73.6 kJ mol^{-1} for the B1-B2 transition under compression at 1.95 GPa and 77.4 kJ mol^{-1} for the B2-B1 transition under decompression at 1.87 GPa.[15] Under rapid compression, the pressure changes with time and so do the activation energies. The question arises about how to understand the role of the pressure-dependent activation energies on the kinetics of B1-B2 phase transition at different compression rates.

In the temperature-induced phase transition under rapid changes in temperature, the concept "effective activation energy" (or similarly, "total activation energy") is introduced to describe the kinetics process of the phase transition as a whole in a temperature range.[31–34] Under the situation of rapid compression, we follow a similar approach and use "effective activation energy" instead of activation energy at P and T to describe the kinetics of the B1-B2 phase transition. We address this in the work below.

II. EXPERIMENTAL DETAILS

Symmetric DAC with 300 μm anvil culets were used for the dynamic experiments. KCl powder with 99.99% purity (Alfa Aesar) was loaded into the sample chamber with a diameter of ~120 μm in a rhenium gasket with an indented thickness of 40–50 μm. A small piece of sodium chloride (NaCl, from Alfa Aesar) and/or gold (Au, from Alfa Aesar) was added as pressure marker.[35,36] After sample loading, the DAC was inserted into a double-diaphragm cap-can assembly and coupled with a piezoelectric drive with the diaphragm and piezoelectric drive in compression and decompression configuration, respectively (Fig. 16 in Ref. 13). *In situ* angle dispersive x-ray diffraction was performed at beamline 16-ID-B, HPCAT, Advanced Photon Source, Argonne National Laboratory. An x-ray beam with wavelength of $\lambda = 0.6199$ Å or 0.6889 Å was focused into a $5 \times 6\ \mu m^2$ (full width at half maximum, FWHM) spot on the sample. Two-dimensional diffraction images were collected continuously throughout the compression process with a PILATUS 1M-F or EIGER 1M prototype detector.[14] For the PILATUS detector, the shortest exposure time was 5 ms with a subsequent readout time of 3 ms (or a total acquire period of 8 ms per image). For the EIGER 1M prototype detector, the exposure time was 1.25 ms with negligible readout time. More details about the dDAC, preload setup, and operating the dDAC and detectors can be found in previous work.[13,14]

Three runs were carried out in the dDAC. The pressures in the sample chamber were measured using the equation of state of NaCl[35] or Au.[36] No pressure transmitting media were used under rapid compression since alkali halides are very soft and negligible stresses were measurable below 5 GPa.[37,38] Figure 1 shows the typical x-ray diffraction patterns under rapid compression with a compression rate of 0.4 GPa/s. The (200) reflection of the B1 phase of NaCl was used for pressure determination. The precision of the pressure determination from NaCl is better than 0.01 GPa due to its small bulk modulus (23.8 GPa).[35] Under rapid compression, the intensity of the (200) reflection of B1-KCl decreases continuously with increasing pressure, while the intensity of the (110) reflection of B2-KCl increases. The change in the relative intensities of the (200) reflection for B1 and the (110) reflection for B2 was used to analyze the transformation extent at P at a given compression rate (k) in the B1-B2 phase transition.

In investigating the B1-B2 transition of KCl under rapid compression, the pressure was changed by linearly changing (ramping) the voltage on the piezoelectric transducer with different ramp rates (Fig. 2). The trapezoid waveform was used at different ramp rates, monitored by an oscilloscope. As an example, Figure 2 shows the relationship between applied voltage and pressure. It should be noted that generally the pressure did not respond linearly with time though the voltage on the transducer was changed linearly. The nonlinear change of pressure should be due to the large volume collapse of the B1-B2 phase transition in the sample

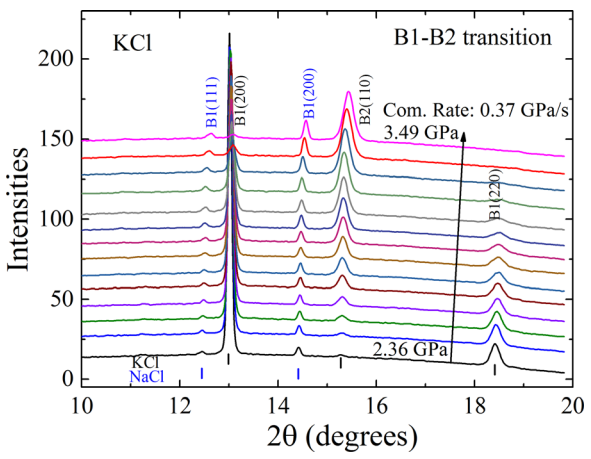

FIG. 1. Typical x-ray diffraction patterns under a compression rate of 0.37 GPa/s with an exposure time of 30 ms for each image. The x-ray wavelength is 0.6889 Å.

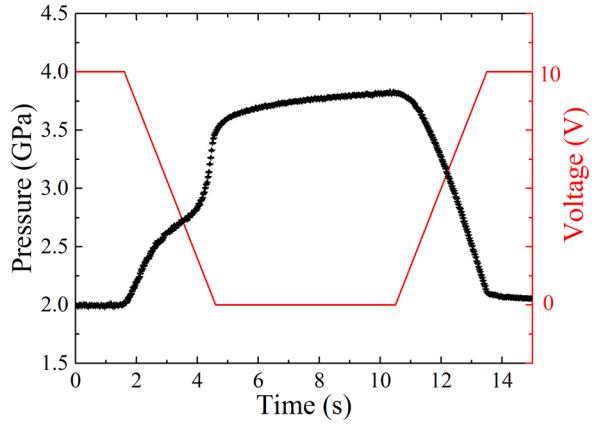

FIG. 2. Ramp compression using the piezoelectric drive system. The Red line and black triangles indicate changes of voltage in piezoelectric drive system monitored by an oscilloscope and sample pressure marked by NaCl,[35] respectively. Note that the piezoelectric actuator was in decompression mode, such that increasing (or decreasing) voltage results in decreasing (or increasing) pressure.

chamber. As shown in Fig. 2, the pressure displays a hump in increasing pressure from ~2.4 GPa to ~3.4 in which a large volume collapse (~12%) occurs during the B1-B2 phase transition, while the pressure decreases almost linearly with time from ~3.8 GP to ~2 GPa because there is no B2-B1 transition which occurs at pressures below 2 GPa in the decompression direction.

Figure 3 shows the representative time dependence of P at various ramp rates under rapid compression. Here, we only present data across the B1-B2 phase transition. The time (t) is normalized by the transition time (t_0) which is defined by a coexistence of the B1 and B2 phases. $t = 0$ is the onset transformation point where the B2 phase was first observed in the x-ray diffraction patterns. For simplicity, we assume that pressure has a linear relationship with time, i.e., $P = k^*t + P_0$, where P_0 is the onset transition pressure and k represents an average compression rate (GPa/s). Then, the overall compression rate (0.03 GPa/s–13.5 GPa/s) was estimated by linearly fitting the determined time-pressure data, as shown in Fig. 3.

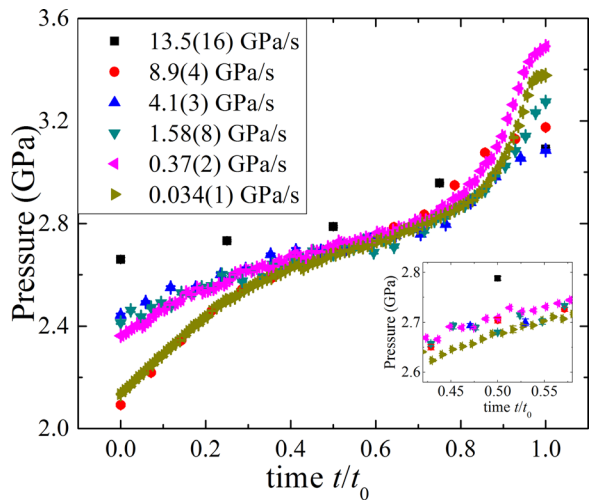

FIG. 3. Representative time-dependent pressure for the B1-B2 phase transition under rapid compression. The time is normalized by the transition time (t_0). The average compression rate was obtained by linearly fitting the data of time and pressure. The exposure time is 300 ms for 0.034 GPa/s; 30 ms for 0.37 GPa/s; and 10 ms for 1.58 GPa/s, 4.1 GPa/s, 8.9 GPa/s, and 13.5 GPa/s. The expanded part around $t/t_0 = 0.5$ is shown in the inset figure.

In addition to x-ray diffraction measurements, we also used fast optical imaging to study the kinetics of B1-B2 phase transition. The pressurized KCl samples are transparent for pure B1 or B2 phases as viewed under a microscope in transmitted light. During the transition process where B1 and B2 coexist, the samples exhibit visible textures due to grain boundaries and domains, as shown in Fig. 4 for the B1-B2 phase transition at a given compression rate. The sample texture and transparency was used to monitor compression-rate dependence of the B1-B2 phase transition in KCl by using a high-speed camera (Photron FASTCAM SA3) at HPCAT. The time resolution was in the range of 0.02–8 ms depending on the compression rates and corresponding exposure time. We used ImageJ software to analyze data and obtain the transition time at different compression rates. The compression rates were estimated to be proportional to $1/\Delta t$, where Δt was the ramping time of the piezoelectric transducer monitored by an oscilloscope. The starting and final pressures were determined by the ruby fluorescence method.[39]

III. MODEL

A first-order phase transition is typically a combined process of nucleation, growth, and impingement. The nucleation and growth rates are related to the activation energies Q_N and Q_G, respectively. At constant P and T, the nucleation and growth rates are regarded to be time independent since Q_N and Q_G are constant. The extent of the phase transformation process (or specifically, the volume fraction of the product phase) as a function of time can be described by the Johnson-Mehl-Avrami-Kolmogorov (JMAK) equation[40–44]

$$f(t) = 1 - \exp[-bt^m], \tag{2}$$

where t is time, $f(t)$ is the volume fraction at time t, b is the rate constant, and m is the growth exponent. Because activation energies are pressure-dependent and can vary with pressure under the rapid compression process, Equation (2) is not suitable to be directly applied under rapid compression. Several theories have been developed based on the classical nucleation and growth theories to explain the kinetics of temperature-induced phase transitions under rapid changes in temperature.[31,32,34,45–48] These theories are not directly applicable for the pressure-induced phase transition because of the different roles of pressure and temperature in the phase transition. Here, we propose a model to analyze and describe the kinetics of phase transitions under rapid compression.

The JMAK equation (Eq. (2)) has been used successfully to describe many experimental results of phase transformation kinetics at constant P and T. In the case of varying P under rapid compression, the volume fraction can be described by[44]

$$f(t) = 1 - \exp[-x_{ex}(t)], \tag{3}$$

where x_{ex}(t) is the extended volume which is determined by nucleation rate I(t) and growth rate v(t)[15,32,44]

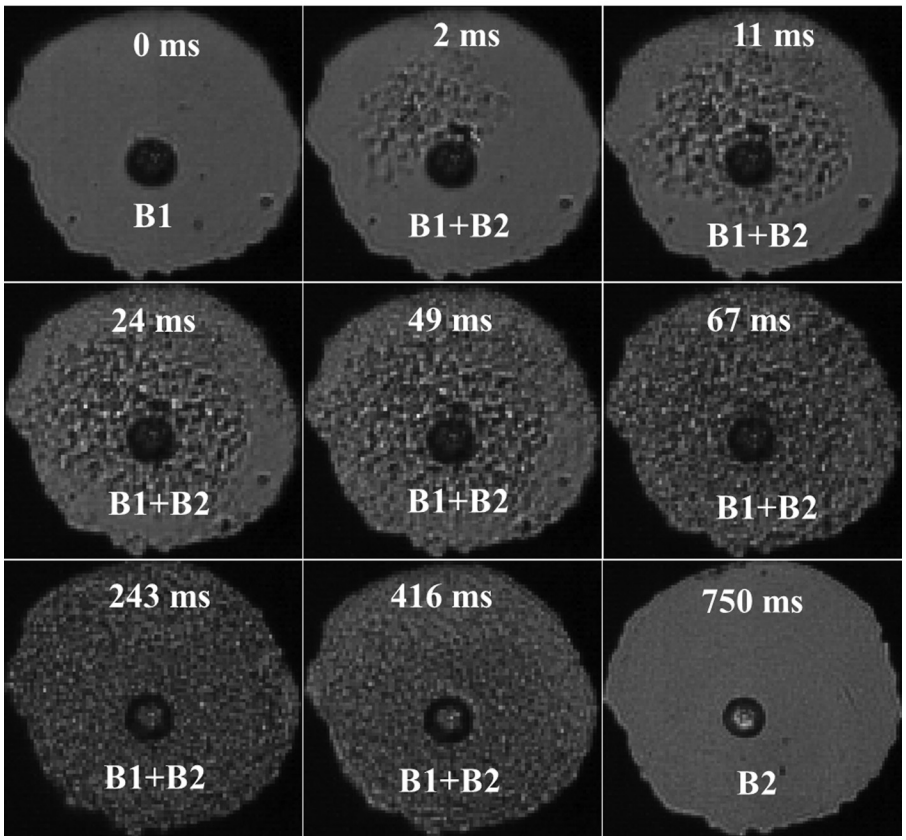

FIG. 4. An example of the B1-B2 transition in KCl using a high-speed camera, with an exposure time of 0.2 ms, showing the textured translucent appearance of the sample during the phase transition process. The dark circle near the center of the sample chamber is a ruby sphere used for pressure measurement. The compression rate was estimated to be 2.4 GPa/s.

$$x_{ex}(t) = \int_0^t I(t)\left[\int_\tau^t v(\tau')d\tau'\right]^n d\tau, \quad (4)$$

$$I(t) = I_0 \exp\left[-(\Delta G_c + Q_N)/k_B T\right], \quad (5)$$

$$v(t) = v_0 \exp\left[-Q_G/k_B T\right]\left[1 - \exp\left(\Delta G_v/k_B T\right)\right], \quad (6)$$

where ΔG_c is the critical energy barrier for nucleation depending on the difference of the Gibbs free energy between the parent and new phases[44] (here, we assume $\Delta G_c \ll k_B T$ because the critical energy barrier decreases dramatically with increase of difference between Gibbs free energies in B1 and B2 phases); Q_N and Q_G are the activation energies in the nucleation and growth processes, respectively; ΔG_v is the difference of the Gibbs free energy induced by the volume change associated with the transformation; k_B is Boltzman constant; T is room temperature (300 K in this study); and n is the growth exponent.[44] At constant P and T, Eqs. (3)–(6) will yield the JMAK equation (2).

Here, we assume that the pressure changes linearly with time (t), i.e., $P = k^* t + P_0$, where P_0 is the onset phase transformation pressure and k is the average compression rate (GPa/s) obtained by fitting pressure-time data (e.g., Fig. 2). Then, we can use P instead of t and obtain the volume fraction as a function of pressure from (3) and (4)

$$f(P) = 1 - \exp[-x_{ex}(P)], \quad (7)$$

$$x_{ex}(P) = k^{-1-n}\int_{P_0}^P I(P)\left[\int_{P'}^P v(P'')dP''\right]^n dP', \quad (8)$$

where nucleation rate $I(P)$ and growth rate $v(P)$ are pressure dependent at a given compression rate. To the first order approximation, we assume that

$$\Delta G_v \approx \Delta V^*(P - P_{tr}), \quad (9)$$

$$Q_N \approx Q_{N0} + \Delta V_N{}^*(P - P_0), \quad (10)$$

$$Q_G \approx Q_{G0} + \Delta V_G{}^*(P - P_0), \quad (11)$$

where ΔV is the volume change of the phase transformation; P_{tr} is the thermodynamic equilibrium pressure where Gibbs free energies between parent and product phases are equal; P_0 is the onset phase transformation pressure where the product phase first occurs; Q_{N0} and Q_{G0} are constant at given compression rate (k); ΔV_N and ΔV_G are the coefficients in the first order approximation. Substituting Equations (9)–(11) into Equations (5), (6), and (8), we obtain

$$\begin{aligned} x_{ex}(P) &= k^{-1-n}\int_{P_0}^P I(P)\left[\int_{P'}^P v(P'')dP''\right]^n dP', \\ &= Ak^{-1-n}\int_{P_0}^P \exp\left[-\frac{\Delta V_N(P' - P_0)}{k_B T}\right] \\ &\quad \times \left[\int_{P'}^P \exp\left[-\frac{\Delta V_G(P'' - P_0)}{k_B T}\right]\right. \\ &\quad \left.\times\left(1 - \exp\left[-\frac{\Delta V(P'' - P_{tr})}{k_B T}\right]\right)dP''\right]^n dP', \quad (12) \end{aligned}$$

$$\text{where } A = (v_0{}^n I_0)\exp\left[-\frac{Q_{N0} + nQ_{G0}}{k_B T}\right]. \quad (13)$$

Here, A is related to activation energy at a given compression rate (k). n is the dimensionality of the growth, the so-called Avrami exponent.[44] Thus, the volume fraction as a

function of pressure depends on the following parameters: A, ΔV, ΔV_G, ΔV_N, n, T, P_{tr}, and P_0 at given compression rate (k). The parameters of ΔV, T, and P_0 can be obtained from experiments. ΔV can be obtained from the volume change ($\sim$6.8 Å^3 per formula) in the phase transition. T is the room temperature ($T = 300$ K). A P_{tr} value of 1.91 GPa is used, which is from the static compression by Hamaya and Akimoto.[15] P_0 can be obtained from experiments (see Fig. 10 below). Then A, n, ΔV_N, and ΔV_G are the only fitting parameters in the model. For homogeneous nucleation and growth, the growth exponent (n) should be equal to 3 when nuclei form in the grain interior and grow along three dimensions.[44] If nuclei form on the grain boundaries and surfaces, nuclei grow along two dimensions and n should be equal to 2, i.e., heterogeneous nucleation.[44] In practice, n could be between 1 and 3 due to the mixture of the different nucleation mechanisms and can be obtained by fitting experimental data. However, Equation (12) is still complicated due to the multiple unknown parameters (A, n, ΔV_N, and ΔV_G). Here, we simplify the model by assuming that ΔV_N is equal to ΔV_G (denoted as $\Delta V_{G,N}$) in the nucleation and growth process, and fixing n to 3, 2, and 1, respectively, leaving only two parameters A, and $\Delta V_{G,N}$ in fitting the volume fraction data according to Equations (7) and (12).

IV. RESULTS AND DISCUSSION

Figure 5 shows the evolution of the (110) reflection of the B2 phase in the B1-B2 phase transition as a function of pressure at various compression rates. Rapid compression on KCl was carried out at different ramp rates in the sequence from high compression rate to low compression rate. Before each compression sequence, diffraction from the B1 phase yielded homogeneous diffraction lines similar to those observed in Fig. 5 for the B2 phase at compression rates of 0.37 GPa/s and 1.58 GPa/s. When a low compression rate of 0.034 GPa/s was applied, spotty patterns of the (110) peak of the B2 phase in diffraction images were observed and then grew with increasing pressure (time). This could be related to grain growth under slow compression rate. The slow compression resulted in large and inhomogeneous diffraction spots, while rapid compression led to homogeneous diffraction rings. The compression-rate dependence in x-ray diffraction images helps to provide constraints on the nucleation and the growth rates of the B1-B2 phase transitions in KCl.

After integrating two-dimensional x-ray diffraction images, we obtain the x-ray diffraction patterns as a function of pressure (time) at given compression rates, as shown in Fig. 1. From this, we can obtain the relative intensities (I_1/I_2) of the (200) reflection of the B1 phase and (110) reflection of the B2 phase in the diffraction pattern. The Bragg diffraction intensity (I) is determined by $I = C_0 * |F(hkl)|^2 * M(hkl) * L * A_{ac} * n_{mol} / V_{unit\ cell}$, where C_0 is a constant including the incident beam intensity, wavelength, and distance between sample and detector; $F(hkl)$ is structure factor for reflection (hkl); $M(hkl)$ is multiplicity, L is Lorentz-polarization factor, A_{ac} is absorption coefficient, n_{mol} is mole number of the phase, $V_{unit\ cell}$ is unit cell volume. Using this diffraction intensity equation, the relative mole number (n_{mol}(B1)/n_{mol}(B2)) can be calculated from the relative intensities (I_1/I_2) of the (200) peak of the B1 phase and (110) peak of B2 phase. The volume fraction of the B2 phase at time (t) is defined by $f(t) = V_2(t)/(V_1(t) + V_2(t))$, where $V_1(t)$ and $V_2(t)$ are the volumes of the B1 and B2 phases at t, respectively. $V_1(t)$ and $V_2(t)$ are equal to n_{mol}(B1)*$V_{unit\ cell}$(B1) and n_{mol}(B2)*$V_{unit\ cell}$(B2). The unit cell volume is obtained from experimental data. Converting from time to pressure, we plot in Fig. 6 the volume fraction $f(P)$ as a function

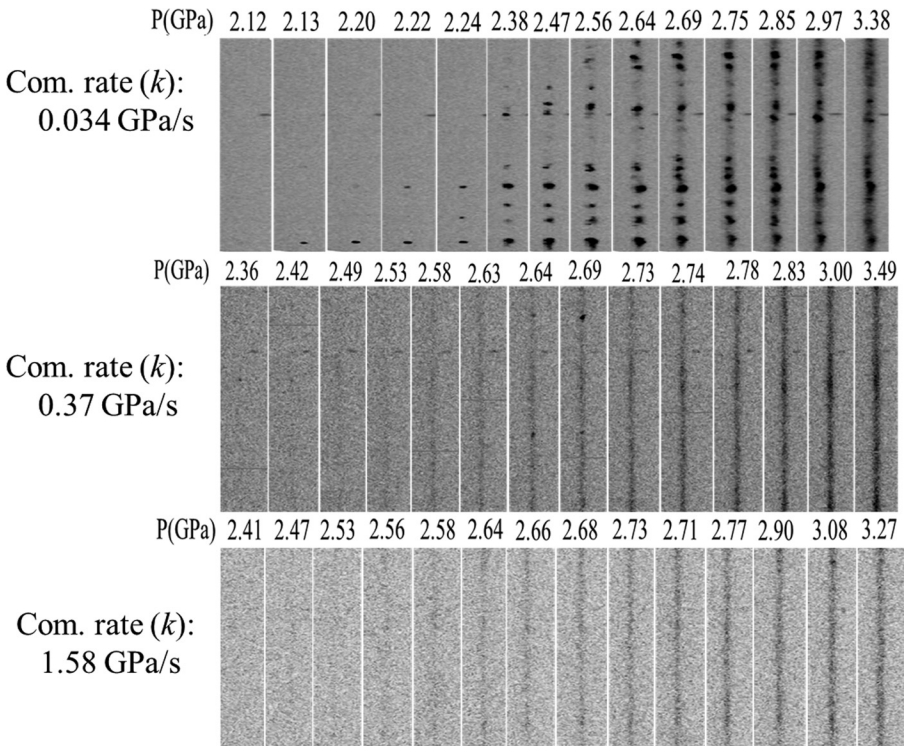

FIG. 5. Pressure (time)-dependent evolution of x-ray diffraction images upon compression qualitatively demonstrates the dependence of the grain size on the compression rates. It is obtained by caking (unrolling) the two-dimensional x-ray diffraction image using Fit2D.[49] The horizontal axis is a narrow range of 2Θ. The vertical axis is azimuth angle for each image at given compression rate and pressure. The compression direction is parallel to the x-ray beam and perpendicular to the azimuth angle.

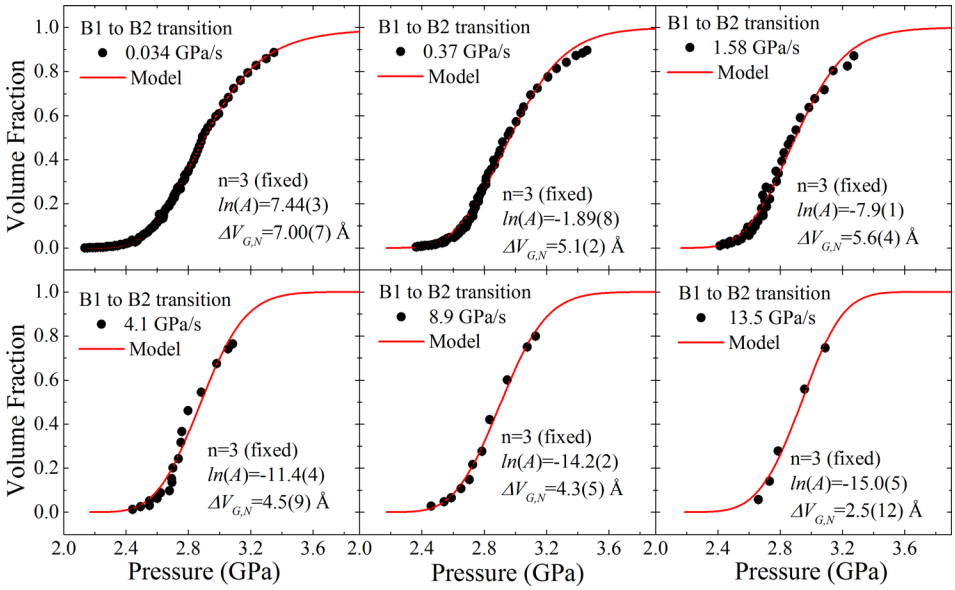

FIG. 6. Volume fraction of the B2 phase as a function of pressure at different compression rates. Black circle symbols show the experimental data. Red lines are the fitting results from Equations (7) and (12) with n = 3 fixed. NaCl was used as pressure marker.

pressure for the B1-B2 transition at different compression rates. It can be seen that the volume fraction generally gives sigmoidal curves for fraction against pressure (or time) under rapid compression, in which the fraction increases slowly at first, then much more rapidly, and finally slowly again.

The experimental data can be well fitted using Eqs. (7) and (12) at low compression rate (0.034 GPa/s) with an R-square value of 0.999, as shown in Fig. 6. At high compression rates (13.5 GPa/s), the fitting results become slightly worse with an R-square value of 0.995. This could be partly due to experimental uncertainties arising from poorer temporal resolution at higher compression rates where we were able to collect only a few data points throughout the transition. The approximations made in the model, such as a first order approximation of activation energy and difference of Gibbs free energy, or the linear change of pressure with time, may be other reasons. Nevertheless, the resultant data from the model provide an interesting general trend of corresponding parameters (A and $\Delta V_{G,N}$) with compression rates with n fixed to 3, 2, and 1. In Fig. 6, we only show the fitting results for n = 3 to facilitate comparison between the different compression rates. The fitting result with n = 2 is comparable to that with n = 3 at low compression rate (0.034 GPa/s). Above 0.034 GPa/s, n = 3 gives a better fitting.

According to Eq. (13), the natural logarithm of A ($-ln(A)$) is proportional to the activation energy ($Q_{N0} + nQ_{G0}$), which means that the trend of $-ln(A)$ may be used to indicate the energy barrier of the phase transition. Figure 7 shows the fitting results of $-ln(A)$ as a function of compression rate. It is found that $-ln(A)$ has a linear relationship with the natural logarithm of compression rate ($ln(k)$) for a given n ($n = 1$, 2, and 3) under rapid compression. With increasing compression rate, the activation energy decreases. For the B1-B2 phase transition, $-ln(A)$ with $n = 2$ has a slightly smaller value than that of $n = 3$ at low compression rate (0.03 GPa/s). This may suggest that the formation of nuclei near the grain boundaries and surfaces has slightly smaller activation energy at low compression rates, and heterogeneous nucleation could occur. This result is in agreement with the findings by Hamaya and Akimoto from static experiments.[15] At high compression rates above 0.4 GPa/s, it can be seen that the activation energy with $n = 3$ is smaller than those with $n = 1$ and $n = 2$, implying that the heterogeneous nucleation is suppressed and homogeneous nucleation is dominant at high compression rates.

Similar to the approach used in studying kinetics of the temperature-induced phase transitions under rapid changes in temperature,[31,32] we define $(Q_{N0} + nQ_{G0})/(n+1)$ as effective activation energy (Q_{eff}). The linear relationship between $-ln(A)$ and $ln(k)$, as shown in Fig. 7, leads to a linear relationship between Q_{eff} and $ln(k)$

$$Q_{eff} = a^* ln(k) + b, \tag{14}$$

where a and b are constants. This relationship implies that Q_{eff} across the transition under rapid compression varies linearly with $ln(k)$. It should be noted that Q_{eff} in Eq. (14) is the total effective activation energy of the nucleation and growth, describing the transition process over the entire range of transition pressure. It may be viewed by $Q_{eff} = \int g_P\, Q(P) dP$,

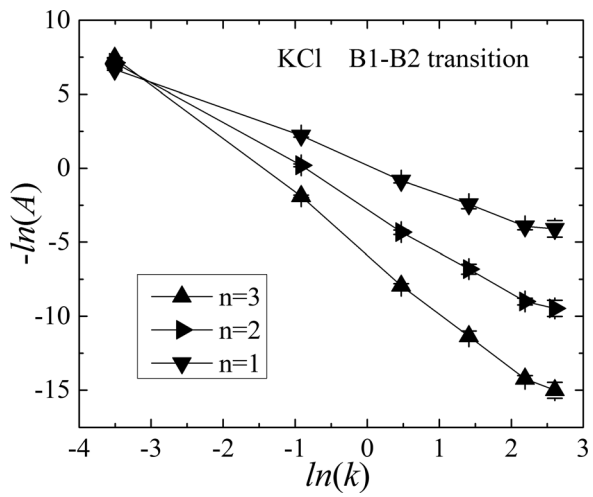

FIG. 7. Relationship between $-ln(A)$) and $ln(k)$. The parameter A is defined in Eq. (13) and related to activation energy at a given k. The unit of k is GPa/s. Uncertainties are shown to be less than or similar to the symbol sizes.

where the integration is over the pressure range of the phase transition, g_P is a weight factor ($0 < g_P < 1$) which is compression-rate dependent, and $Q(P)$ is the average activation energy for nucleation and growth at P and is compression-rate independent. With increasing compression rate, Q_{eff} is inversely proportional to $ln(k)$.

Another parameter obtained from the model is $\Delta V_{G,N}$ which is analogous to activation volume (see Eqs. (10) and (11)). As shown in Fig. 8, $\Delta V_{G,N}$ values are positive and display a general trend of decreasing with increasing compression rates. We note that $\Delta V_{G,N}$ should be viewed as a total averaged parameter that is analogous to average activation volume across the entire phase transition. With the limited experimental data and associated uncertainties, two different relationships are assumed in fitting the $\Delta V_{G,N} - k$ data. The red dashed line in Fig. 8 is the fitted result by assuming a linear relationship between $ln(\Delta V_{G,N})$ and $ln(k)$, while the blue dot line is a linear fit between $\Delta V_{G,N}$ and k. We will show later that these two relations can be constrained using the data of over-pressurization.

The effective activation energy (Q_{eff}) and the averaged activation volume ($\Delta V_{G,N}$) can be used for understanding the experimental observables of the characteristic transition time, the nucleation and growth, and the over-pressurization across the phase transition at various compression rates.

Under rapid compression, the transition time is found to decrease with increasing compression rate. Here, the transition time is defined by the time during which the B1 and B2 phases coexist at a given compression rate (k), with half of the transition time referred to as the characteristic time (τ) of the B1-B2 transition. Fig. 9 shows the relationship between $ln(\tau)$ and $ln(k)$ obtained from both the time-resolved x-ray diffraction and high-speed imaging experiments. Data from two different techniques are consistent with each other. We find an approximately linear decrease of $ln(\tau)$ with $ln(k)$.

According to Eq. (14), Q_{eff} across the phase transition under rapid compression is linearly related to $ln(k)$. If we apply Q_{eff} to the Arrhenius equation (Eq. (1)), the linear

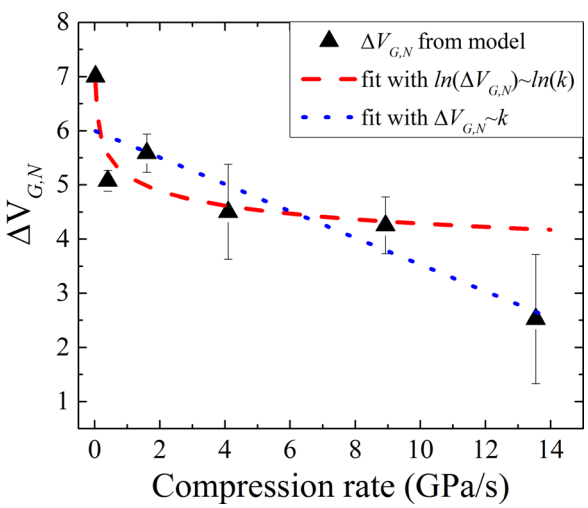

FIG. 8. $\Delta V_{G,N}$ as a function of compression rates. Black triangles represent results by fitting the volume fractions in Fig. 6 with n fixed at 3. The red dashed line is the fitted result assuming a linear relationship between $ln(\Delta V_{G,N})$ and $ln(k)$. The blue dotted line is a linear fit between $\Delta V_{G,N}$ and k.

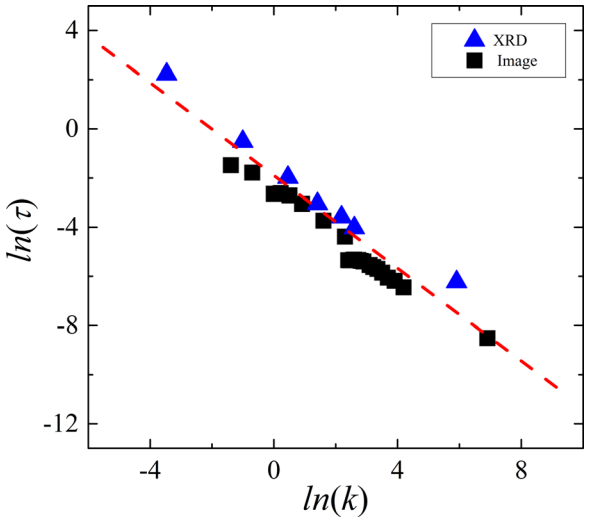

FIG. 9. The relationship between characteristic time (τ, in second) and compression rate (k, in GPa/s). The natural logarithm of τ and k are used. Black squares represent the data from high-speed imaging experiments. Blue triangles are from x-ray diffraction experiments under rapid compression. The red dashed line is a guide for eye.

relationship in Fig. 9 can then be derived from Eq. (1). This applicability of Q_{eff} suggests that the overall activation energy of the B1-B2 transition in KCl under rapid compression may be reasonably well represented by $Q_{eff}(k)$ which is compression rate dependent according to Eq. (14).

Nucleation rate is proportional to $\exp[-Q_N/k_BT]$ and $Q_N \approx Q_{N0} + \Delta V_N^*(P - P_0)$ (Eq. 10). Using Q_{eff} instead of Q_{N0}, we can estimate the nucleation rate at various compression rates. Qualitatively, because Q_{eff} decreases linearly with increasing $ln(k)$, nucleation rate may increase linearly with increasing compression rates at the onset transition pressure, which is in qualitative agreement with the observations shown in Fig. 5. On the other hand, it should be noted that the activation energy for heterogeneous nucleation ($n = 2$) is close to the value for homogeneous nucleation at low compression rate, or it could even be smaller than homogeneous nucleation. This means that heterogeneous nucleation can be more likely to occur on the grain boundary and surface and be competitive with homogeneous nucleation ($n = 3$). This is consistent with the static data by Hamaya and Akimoto.[15] With increasing compression rate, the effective activation energy for homogeneous nucleation decreases, which results in the increasing likelihood of the homogeneous nucleation in the grain interior and suppression of heterogeneous nucleation. At this time, the effect of the grain boundary which may have small activation energy for the formation of nucleation for the B2 phase can be neglected.

Figure 10 shows the onset transition pressure, signified by the first appearance of the B2 phase, as a function of the compression rate. The over-pressurization can be divided into two stages, namely, a steep initial increase at low k and slight increase (or even plateau) at larger k. It indicates that the over-pressurization is small at low compression rate but increases rapidly. Above 0.4 GPa/s, the over-pressurization is large but increases slowly with increasing compression rates. Interestingly, these experimental observations provide a good test of the relationship between activation volume

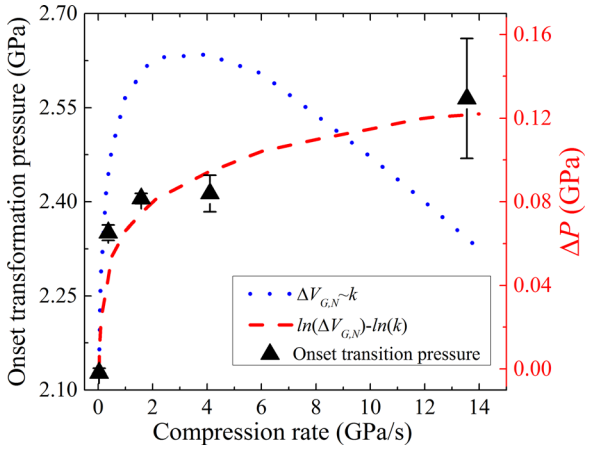

FIG. 10. The over-pressurization effect reflected by the onset phase transformation pressures at various compression rates (k). Black triangles are experimental results from this study. Lines represent the transition pressure changes (ΔP, in GPa) according to the model with the parameter A, as shown in Fig. 7, and the fitted results of $\Delta V_{G,N}$, as shown in Fig. 8. The red dashed line is from the assumption of a linear relationship between $ln(\Delta V_{G,N})$ and $ln(k)$, while the blue dotted line is from a linear relationship of $\Delta V_{G,N} \sim k$.

and the compression rate. As shown in Fig. 8, we are unable to conclusively determine the relationship between $\Delta V_{G,N}$ and k, specifically, whether a relationship between $ln(\Delta V_{G,N})$ and $ln(k)$ holds, or rather a simple relationship between $\Delta V_{G,N}$ and k is appropriate. However, these two relations provide a stark contrast for over-pressurization. Our experimental results on over-pressurization clearly favor a linear relationship between $ln(\Delta V_{G,N})$ and $ln(k)$, as shown in Fig. 10.

V. CONCLUSION

In summary, kinetics of the B1-B2 phase transition in KCl has been investigated under rapid compression in a dynamic diamond anvil cell using time-resolved x-ray diffraction and fast imaging. Based upon JMAK theories, a model is proposed to fit the experimental data of the volume fraction which has sigmoidal curves as a function of pressure (or time). The resulting parameters provide information on the effective activation energy Q_{eff} and the average activation volume $\Delta V_{G,N}$ as a function of compression rate. It is demonstrated that Q_{eff} and $\Delta V_{G,N}$ can be used for interpreting several experimental observations such as compression-rate dependent transition time and over-pressurization. Via fitting, it is concluded that Q_{eff} has a linear relationship with the logarithm of compression rate. This can be used to interpret the experimentally observed linear relationship between the logarithm of transition time and the logarithm of the compression rates. The experimentally observed over-pressurization as a function of compression rate can be simulated from the model when a linear relationship between $ln(\Delta V_{G,N})$ and $ln(k)$ is assumed.

ACKNOWLEDGMENTS

This work was performed at HPCAT (Sector 16), Advanced Photon Source (APS), Argonne National Laboratory. HPCAT operations are supported by DOE-NNSA under Award No. DE-NA0001974 and DOE-BES under Award No. DE-FG02-99ER45775, with partial instrumentation funding by NSF. The Advanced Photon Source is a U.S. Department of Energy (DOE) Office of Science User Facility operated for the DOE Office of Science by Argonne National Laboratory under Contract No. DE-AC02-06CH11357. We are grateful to Dr. Przemyslaw Dera for modifying his GSE-shell code to enable data analysis presented in this work. The authors wish to thank DECTRIS for providing EIGER 1M prototype, and we appreciate the assistance of Matthew Moore, Russell Woods, and Timothy Madden of the APS Detector Pool in facilitating its installation at the beamline.

[1]G. W. Lee, W. J. Evans, and C. S. Yoo, PNAS **104**, 9178 (2007).
[2]J. Y. Chen and C. S. Yoo, PNAS **108**, 7685 (2011).
[3]J. Y. Chen, M. Kim, C. S. Yoo, H. P. Liermann, and W. J. Evans, J. Phys: Conf. Ser. **500**, 142006 (2014).
[4]S. Nemat-Nasser and J. Y. Choi, Acta Mater. **53**, 449 (2005).
[5]S. Nemat-Nasser, J. Y. Choi, W. G. Guo, and J. B. Isaacs, Mech. Mater. **37**, 287 (2005).
[6]D. A. Tomasino and C. S. Yoo, J. Phys: Conf. Ser. **500**, 032019 (2014).
[7]N. Velisavljevic, S. Sinogeikin, R. Saavedra, R. S. Chellappa, A. Rothkirch, D. M. Dattelbaum, Z. Konopkova, H. P. Liermann, M. Bishop, G. M. Tsoi, and Y. K. Vohra, J. Phys: Conf. Ser. **500**, 032020 (2014).
[8]D. Tomasino and C. S. Yoo, Appl. Phys. Lett. **103**, 061905 (2013).
[9]J. Y. Chen and C. S. Yoo, J. Chem. Phys. **136**, 114513 (2012).
[10]J. Y. Chen, C. S. Yoo, W. J. Evans, H. P. Liermann, H. Cynn, M. Kim, and Z. Jenei, Phys. Rev. B **90**, 144104 (2014).
[11]W. J. Evans, C. S. Yoo, G. W. Lee, H. Cynn, M. J. Lipp, and K. Visbeck, Rev. Sci. Instrum. **78**, 073904 (2007).
[12]S. Q. Chu, L. R. Zheng, Y. L. Zhou, A. Y. Zhou, J. Zhang, R. Z. Che, J. Liu, and T. D. Hu, J. Synchrotron Rad. **18**, 728 (2011).
[13]S. V. Sinogeikin, J. Smith, E. Rod, C. Lin, C. Kenney-Benson, and G. Shen, Rev. Sci. Instrum. **86**, 072209 (2015).
[14]J. S. Smith, S. Sinogeikin, C. L. Lin, E. Rod, and G. Shen, Rev. Sci. Instrum. **86**, 072208 (2015).
[15]N. Hamaya and S. Akimoto, High Temp. - High Pressures **13**, 347 (1981).
[16]S. Froyen and M. L. Cohen, J. Phys. C: Solid State Phys. **19**, 2623 (1986).
[17]S. N. Vaidya and G. C. Kennedy, J. Phys. Chem. Solids **32**, 951 (1971).
[18]P. W. Bridgman, Proc. Am. Acad. Arts Sci. **76**, 1 (1945).
[19]W. A. Bassett, T. Takahashi, and J. K. Campbell, Trans. Am. Crystallogr. Assoc. **5**, 93 (1969).
[20]T. Kinoshita, T. Mashimo, and K. Kawamura, J. Phys.: Condens. Matter **17**, 1027 (2005).
[21]D. B. Hayes, J. Appl. Phys. **45**, 1208 (1974).
[22]T. d'Almeida and Y. M. Gupta, Phys. Rev. Lett. **85**, 330 (2000).
[23]T. Mashimo, K. Nakamura, K. Tsumoto, Y. Zhang, S. Ando, and H. Tonda, J. Phys.: Condens. Matter **14**, 10783 (2002).
[24]S. J. Turneaure, Y. M. Gupta, and P. Rigg, J. Appl. Phys. **105**, 013544 (2009).
[25]E. Zaretsky, J. Phys. Chem. Solids **59**, 253 (1998).
[26]T. Kinoshita, T. Mashimo, and K. Kawamura, J. Appl. Phys. **101**, 093517 (2007).
[27]N. V. C. Shekar and K. G. Rajan, Bull. Mater. Sci. **24**, 1 (2001).
[28]A. K. Singh, Bull. Mater. Sci. **5**, 219 (1983).
[29]A. K. Singh, Mater. Sci. Forum **3**, 291 (1985).
[30]S. Glasstone, K. J. Laidler, and H. Eyring, *The Theory of Rate Processes* (McGraw-Hill, New York, 1941).
[31]J. Farjas and P. Roura, Acta Mater. **54**, 5573 (2006).
[32]F. Liu, F. Sommer, C. Bos, and E. J. Mittemeijer, Int. Mater. Rev. **52**, 193 (2007).
[33]A. K. Rai, S. Raju, B. Jeyaganesh, E. Mohandas, R. Sudha, and V. Ganesan, J. Nucl. Mater. **383**, 215 (2009).
[34]S. Raju and E. Mohandas, J. Chem. Sci. **122**, 83 (2010).
[35]F. Birch, J. Geophys. Res. **91**, 4949, doi:10.1029/JB091iB05p04949 (1986).
[36]O. L. Anderson, D. G. Isaak, and S. Yamamoto, J. Appl. Phys. **65**, 1534 (1989).

[37]G. J. Piermarini, S. Block, and J. D. Barnett, J. Appl. Phys. **44**, 5377 (1973).
[38]K. Asaumi and A. L. Ruoff, Phys. Rev. B **33**, 5633 (1986).
[39]H. K. Mao, J. Xu, and P. M. Bell, J. Geophys. Res. **91**, 4673, doi:10.1029/JB091iB05p04673 (1986).
[40]W. A. Johnson and R. F. Mehl, Trans. Am. Inst. Min. (Metal.) Eng. **135**, 416 (1939).
[41]M. Avrami, J. Chem. Phys. **7**, 1103 (1939).
[42]M. Avrami, J. Chem. Phys. **8**, 212 (1940).
[43]M. Avrami, J. Chem. Phys. **9**, 177 (1941).
[44]J. W. Christian, *The Theory of Transformation in Metals and Alloys* (Pergamon Press, Oxford, Oxford, 2002).
[45]P. J. Skrdla, J. Phys. Chem. Solids **74**, 1375 (2013).
[46]G. Ruitenberg, E. Woldt, and A. K. Petford-Long, Thermochim. Acta **378**, 97 (2001).
[47]E. Woldt, J. Phys. Chem. Solids **53**, 521 (1992).
[48]P. Kruger, J. Phys. Chem. Solids **54**, 1549 (1993).
[49]A. P. Hammersley, S. O. Svensson, M. Hanfland, A. N. Fitch, and D. Hausermann, High Press. Res. **14**(4–6), 235 (1996).